Sommerfeld expansion of electronic entropy in an INFERNO-like average atom model

Philippe Arnault [ORCID],[*] Julien Racine, and Jean-Pierre Raucourt
CEA, DAM, DIF, F-91297 Arpajon, France

Augustin Blanchet [ORCID] and Jean-Christophe Pain [ORCID]
CEA, DAM, DIF, F-91297 Arpajon, France
and Université Paris-Saclay, CEA, Laboratoire Matière en Conditions Extrêmes, 91680 Bruyères-le-Châtel, France

In the average atom (AA) model, the entropy provides a route to compute thermal electronic contributions to the equation of state (EOS). The complete EOS comprises in many modelings an additional 0 K isotherm and a thermal ionic part. Even at low temperature, the AA model is believed to be the best practical approach. However, when it comes to determining the thermal electronic EOS at low temperatures, the numerical implementation of AA models faces convergence issues related to the pressure ionization of bound states. At contrast, the Sommerfeld expansion tells us that the variations with temperature of thermodynamic variables should express in simple terms at these low temperatures. This led us to tackle the AA predictions with respect to the Sommerfeld expansion of the electronic entropy. We performed a comprehensive investigation for various chemical elements belonging to s, p, d, and f blocks of the periodic table, at varying densities. This was realized using an INFERNO-like model since this approach provides the best theoretical framework to address these issues. We found that the Sommerfeld expansion is valid for a ratio of the temperature to the Fermi energy of <0.05. This allows us to extend the study to other atomic numbers at a low enough unique temperature. Comparing the AA results with the free electron gas model, the discrepancies are $<10\%$ at very high densities but can reach an order of magnitude at the metal-insulator transition.

I. INTRODUCTION

The equation of state (EOS) relates the state variables of a material: pressure, temperature, internal energy, and so on. It also delineates the frontiers of the solid, liquid, gas, and plasma phases [1]. For these reasons, the EOS contributes to the foundation of various process engineering, technological applications, and astrophysics. Furthermore, the study of matter under extreme conditions is crucial for the understanding of the physics of stellar and planetary interiors as well as for the design and interpretation of inertial confinement fusion (ICF) experiments [2]. The ICF modeling consists of hydrodynamic simulations requiring reliable EOS data for a variety of elements over a wide range of material conditions, from the solid state to the rarefied plasma and high-energy-density regimes [3]. The large range of conditions and their extreme nature make it impossible to completely explore the EOS experimentally, and thus, theoretical modelings, benchmarked against experiments at selected density-temperature conditions, are determinant [4]. The most accurate theoretical approaches consist of *ab initio* simulations within density functional theory (DFT) [5,6] or path integral Monte Carlo formalism [7]. Unfortunately, these techniques are so computationally demanding that they are often viewed as scarce, albeit essential [8]. Since the hydrodynamics requires stringent constraints of conservation of mass,

momentum, and energy [9], EOS approximations often come along with a free energy model, which warrants thermodynamic consistency. In this context, the average atom (AA) model has become instrumental (see Ref. [10] and references therein).

EOS models typically consist of three parts: the cold curve, the ion-thermal contribution, and the electron-thermal contribution [11]. This separation aims at taking the best from the theoretical models for each contribution. AA models are used for the electron-thermal part [12], whereas the cold curve benefits from experimental measurements and is guided by solid state physics [13]. The ion-thermal contribution considers experiments at low temperature but must also reproduce the wide-range behavior from the solid and liquid up to more or less correlated plasmas [14–16].

In this paper, we focus on the AA predictions in the low-temperature regime, characteristic of solids and liquid metals. Measuring the pressure in compressed matter can constrain the cold curve (0 K isotherm), whereas the thermal contribution is often constrained by other measurements—heat capacity, for instance. When compared with EOS modeling, this thermal contribution is dominated by the ion motion with a small part due to electron excitation [1]. Therefore, the modeler is left alone with theoretical tools. A quick look at the literature about the multiphase EOS shows that there is no consensus for the best way to account for the electron-thermal contribution. Simple prescriptions rest on the free electron gas (FEG) model using the Thomas-Fermi (TF) ionization [17] or some Sommerfeld-like approximation where

thermodynamic quantities are expressed as power laws in temperature and density [18]. More involved prescriptions use the TF AA model [18–22] or its quantum-mechanical extensions [18,23] before resorting to *ab initio* simulations [24]. Although the AA model is considered the most realistic of the practical approaches, it faces convergence issues at low temperature when pressure ionization of the fully occupied bound state occurs [25]. This is to be contrasted with the simplicity of the Sommerfeld expansion of thermodynamic variables in powers of the temperature [26–28].

Here, we contribute to the modeling of the electron-thermal EOS at low temperature using an INFERNO-like AA model [29–31] to compare its predictions with the Sommerfeld approximation. This kind of AA model, which derives variationally from a free energy functional, is recognized as one of the best approaches to tackle the pressure ionization of bound states into resonances, which extend the representation of localized charge from the spectrum of bound states to the free energy continuum [25]. This avoids the appearance of discontinuities of thermodynamic variables and allows us to compare them with their Sommerfeld expansion. Of particular importance for the thermodynamic consistency is the treatment of both bound and free states on the same footing. As a result, there is no band structure at low temperature as in solid state physics due to the absence of spatial periodicity. Some other AA models [32–34] incorporate a kind of canonical band enlarging the bound states at the expense of breaking the symmetric treatment with free states.

We extensively studied four elements: hydrogen, aluminum, iron, and cerium, which belong to *s*, *p*, *d*, and *f* blocks of the periodic table. For selected conditions, we also included a larger range in atomic number *Z*. Furthermore, we chose to work with the electronic entropy since it easily provides the thermal EOS, as explained in Appendix A, and is straightforwardly related to the density of states (DOS). We also chose the entropy as a route toward the thermal contribution to avoid numerical inaccuracy inherent in the differences between larger numbers representative of the internal energy and the pressure evaluated at finite temperature and 0 K.

In a first theoretical part, we briefly recall the tenets of the AA modeling in Sec. II A to set the problems of pressure ionization and to introduce the relevant quantities. We also go into the detail on the Sommerfeld approximation in Sec. II B and present a direct Sommerfeld-like approach to the electronic entropy in Sec. II C. This theoretical part ends in Sec. II D by a presentation of the FEG model as a useful concept in the present context.

The results of an INFERNO-like model are described in Sec. III for hydrogen (Sec. III A), aluminum (Sec. III B), iron (Sec. III C), and cerium (Sec. III D) in a large range of density from 10^{-4} to 10^4 g. cm^{-3} at low temperature from 0.01 to 10 eV. They are further analyzed in Sec. IV where the domain of validity of the Sommerfeld approximation is delineated (Sec. IV A). This analysis allowed us to extend the study to a larger set of elements to evidence any trends with the atomic number *Z* (Sec. IV B). The FEG model is shown to be adequate for very dense systems only (Sec. IV B 2). Finally, the sensitivity of the results to the exchange-correlation (XC) functional is addressed in Sec. IV C.

II. THEORY

A. INFERNO-like AA

The principle behind the AA modeling is to represent the many-body system of electrons and nuclei by an equivalent unique atom submitted to appropriate boundary conditions [10]. The most obvious constraint to confine the AA is a volume *V* related to the mass density ρ of the medium. Many models differ in the way this confinement is realized [29,35–39]. The most simple one, used in INFERNO, involves the Wigner-Seitz (WS) sphere of radius r_{ws} given by

$$\frac{4}{3}\pi r_{\text{ws}}^3 n_i = 1, \tag{1}$$

where $n_i = \rho N_A/A$ is the number density, *A* the molar mass of the chemical element, and N_A the Avogadro number. The constraint states that the volume $V = 1/n_i$ containing the AA should be neutral.

The electronic structure of this atom is computed within the framework of DFT [40–43]. This leads to an AA with fractional occupancy n_s of the bound states ε_s equal to the product of their degeneracy g_s by the Fermi-Dirac (FD) function $f(\varepsilon_s)$:

$$n_s = g_s f(\varepsilon_s), \tag{2}$$

where *s* stands for the principal quantum number *n*, and the quantum numbers *j*, ℓ, and *m* are associated respectively with the total angular momentum *J*, the orbital angular momentum *L*, and its projection L_z. The same is true for free states except that the index *s* stands for the energy ε, or the wave vector *k*, instead of the principal quantum number *n*.

The INFERNO model proposes a consistent framework where the equations were obtained through the minimization of a free-energy functional [29–31]. This warrants *a priori* the thermodynamic consistency of the results. The model considers an atom as a point nucleus surrounded by its *Z* electrons and places it at the center of the WS spherical cavity buried in a jellium, i.e., a uniform distribution of positive charges which takes the place of the surrounding ions, and a constant electron distribution that ensures electrical neutrality. The electronic structure is then computed in a self-consistent way, where the effective potential $V_{\text{eff}}(\vec{r})$ within the cavity is a functional of the electron density $n_e(\vec{r})$ itself computed from the wave functions subject to the effective potential. Outside the cavity, the latter is assumed to be constant.

Every electron is represented by a wave function $\psi_s(\vec{r})$ that is a solution of the Dirac equation, with exponentially decreasing boundary conditions at large distance for bound states and oscillating behavior for free states. In the WS sphere, the effective potential $V_{\text{eff}}(r)$ is spherically symmetric, and the wave function ψ_s is composed of two radial components, the major component $F_s(r)$ and the minor one $G_s(r)$, in contrast to the radial Schrödinger equation that only needs one. These radial components are solutions to the following system of equations [44]:

$$\frac{dF_s}{dr} = -\frac{\kappa_s}{r}F_s(r) - \frac{1}{c}[V_{\text{eff}}(r) - c^2 - \varepsilon_s]G_s(r),$$

$$\frac{dG_s}{dr} = +\frac{\kappa_s}{r}G_s(r) + \frac{1}{c}[V_{\text{eff}}(r) + c^2 - \varepsilon_s]F_s(r), \tag{3}$$

where atomic units (a.u.) $e = \hbar = m_e = 1$ are used, and we choose to keep the speed of light *c* instead of the hyperfine

structure constant α. The orbital parameter κ_s is

$$\kappa_s = \begin{cases} -(\ell+1) & \text{if } j = \ell + \frac{1}{2}, \\ +\ell & \text{if } j = \ell - \frac{1}{2}. \end{cases} \quad (4)$$

Inside the cavity, the effective potential V_{eff} comprises the interaction with the nucleus of charge Z, the electrostatic interaction with the total electron density n_e, and the XC potential V_{xc}:

$$V_{\text{eff}}(r) = -\frac{Z}{r} + \int_{r' \leqslant r_{\text{ws}}} \frac{n_e(r')}{|\vec{r} - \vec{r}\,'|} d^3\vec{r}\,' + V_{\text{xc}}(r). \quad (5)$$

One of the numerical challenges in the solution of these equations concerns the dissolution of bound states within the continuum of free states as the density increases. This phenomenon, known as *pressure ionization*, leads to particular issues at low temperature when the bound states are completely occupied since the large localized density associated with the bound state cannot abruptly transit to a situation of complete delocalization. Instead, the solution exhibits sharp resonances in the continuum that are the scars of the disappearing bound states. As the compression goes on increasing, these resonances enlarge and progressively dissolve into the continuum. The detection and the discretization of these resonances represent a cumbersome numerical challenge.

The electronic structure (bound and free states) being known, the thermodynamic quantities can be calculated. A theoretical issue then shows up that is best explained by Liberman [29]: "In devising this model of condensed matter, where a single atom is embedded in an electron gas, we introduced the electron gas to simulate the effects of the surrounding atoms on a particular one. However, it is the properties of the atom—its energy, for example—which concern us. However, the mathematical expressions for these quantities include large contributions from the electron gas." To circumvent this issue, Liberman proposed two main versions of INFERNO: the so-called A and T models, differing by the calculation of thermodynamic quantities. In the T model, the quantities related to the jellium are subtracted from the quantities calculated in the whole space, whereas in the A model, the separation between the ionic cell and the jellium is of spatial nature. For instance, the PURGATORIO code [30] is very close to the A model. Liberman's model A states that thermodynamic quantities must be either obtained from integrations limited to the WS confinement sphere or multiplied by the factors $X(\varepsilon_s)$, giving the fraction of the density, associated with the wave function ψ_s, pertaining to the confinement volume:

$$X(\varepsilon_s) = \int_{r \leqslant r_{\text{ws}}} \psi_s(\vec{r})\, \psi_s^*(\vec{r})\, d^3r,$$

$$= 2\,|\kappa_s| \int_0^{r_{\text{ws}}} \left[F_s^2(r) + G_s^2(r) \right] dr. \quad (6)$$

This model-dependent prescription represents a step outside a thermodynamic consistent framework, but this is the price to connect quantities obtained from the AA to quantities representative of the whole system. It is expected that inconsistency may appear when $f(\varepsilon_s) \sim 1$ and $X_s \ll 1$. Unfortunately, this happens during the transition from bound states toward sharp resonances. In this situation, the bound wave function extends

outside the WS sphere, but the overlapping with the corresponding wave-functions of neighboring atoms, which would lead to the formation of a band structure, is neglected. Since the model is precisely built to address this kind of issue, it is only *a posteriori* that a consistency check can be performed.

In the following, we shall need to consider the DOS $n(\varepsilon)$ and the entropy S per atom given respectively by

$$n(\varepsilon) = \frac{1}{V} \left[\sum_{s\,\text{bound}} \delta(\varepsilon - \varepsilon_s) + H(\varepsilon - V_\infty) \right] X(\varepsilon), \quad (7)$$

where H is the Heaviside function, δ the Dirac distribution, and

$$\frac{S}{V} = -k_B \int_{-\infty}^{+\infty} n(\varepsilon)\, s(\varepsilon)\, d\varepsilon + \frac{S_{\text{xc}}}{V}, \quad (8)$$

where

$$s(\varepsilon) = f(\varepsilon) \ln f(\varepsilon) + [1 - f(\varepsilon)] \ln [1 - f(\varepsilon)], \quad (9)$$

and S_{xc} comes from the XC free energy functional. This contribution to the XC is important in partially degenerate plasmas but can be safely neglected at the low temperatures where the Sommerfeld expansion is valid (see fig. 1 in Ref. [45]). As we shall see in Sec. IV, the validity domain of Sommerfeld's approximation has an upper limit in the degeneracy parameter $\theta = k_B T / \varepsilon_F$ of the order of 0.05 [see Eq. (35) for the definition of the Fermi energy ε_F]. As evaluated in Sec. IV C, the XC entropy S_{xc} is a small contribution in this range of θ values.

It is instructive to discuss the behavior of the function $s(\varepsilon)$ at low temperature. As Fig. 1 shows, it vanishes wherever ε differs from the chemical potential μ by a few $k_B T$. Therefore, the entropy S is built upon from the values of the DOS $n(\varepsilon)$ in the vicinity of the chemical potential μ. At the same time, the value of the chemical potential μ is determined from the neutrality of the WS confinement sphere. Let us anticipate the definition of $n(\varepsilon)$ in Eq. (23):

$$\frac{Z}{V} = \int_{-\infty}^{\infty} n(\varepsilon) f(\varepsilon)\, d\varepsilon. \quad (10)$$

B. Sommerfeld expansion

Kohn-Sham (KS) DFT describes an equilibrium situation where the electrons can be treated as independent particles moving in an effective potential $V_{\text{eff}}(\vec{r})$ that depends on their density $n_e(\vec{r})$. At finite temperature T [42], the energy levels ε of electrons are occupied according to the FD statistics $f(\varepsilon)$ which involves the inverse temperature $\beta = 1/k_B T$ and the chemical potential μ [27]:

$$f(\varepsilon) = \frac{1}{\exp\left[\beta(\varepsilon - \mu)\right] + 1}. \quad (11)$$

Therefore, the density n_e, as any functional of it, depends explicitly on temperature through the FD function $f(\varepsilon)$. This function is a Heaviside $H(\varepsilon_F - \varepsilon)$ at $T = 0$, transiting from 1 to 0 at the Fermi energy ε_F, which is defined as the highest energy level occupied by electrons at $T = 0$. As the temperature T increases from 0, the steplike jump is located at the value of the chemical potential μ and smooths out over a range of
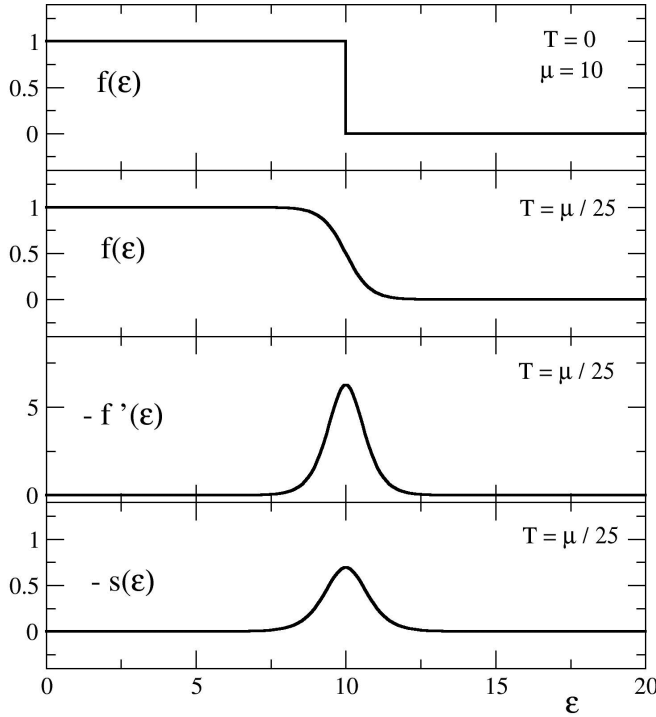
FIG. 1. Behavior of the Fermi-Dirac distribution $f(\varepsilon)$ at low temperature. For the sake of clarity, we choose a temperature $T = \mu/25$ close to the highest temperatures where the Sommerfeld expansion is valid. Also shown are the derivative of $f(\varepsilon)$ and the entropy factor $s(\varepsilon)$. They are sharply peaked and symmetric around μ.

$k_B T$ around μ, as illustrated in Fig. 1. At high enough temperature, the FD function $f(\varepsilon)$ tends to the Maxwell-Boltzmann distribution.

Sommerfeld expansion [26,27] is a low-T Taylor series of integrals of the form:

$$I(T, \mu) = \int_{-\infty}^{\infty} g(\varepsilon) f(\varepsilon) \, d\varepsilon, \quad (12)$$

where $g(\varepsilon)$ is a function vanishing as $\varepsilon \to -\infty$ and diverging no more rapidly than some power of ε as $\varepsilon \to +\infty$. Introducing the primitive $G(\varepsilon)$:

$$G(\varepsilon) = \int_{-\infty}^{\varepsilon} g(\varepsilon') \, d\varepsilon', \quad (13)$$

an integration by part gives

$$I(T, \mu) = -\int_{-\infty}^{\infty} G(\varepsilon) f'(\varepsilon) \, d\varepsilon, \quad (14)$$

with

$$-f'(\varepsilon) = -\frac{\partial f}{\partial \epsilon} = \beta f(\varepsilon)[1 - f(\varepsilon)]. \quad (15)$$

As depicted in Fig. 1, the derivative of the FD distribution $f(\varepsilon)$ is sharply peaked at the value of the chemical potential μ at low temperature ($\theta \ll 1$). The integral $I(T, \mu)$ and its approximations are therefore highly sensitive to the Taylor expansion of $G(\epsilon)$ around $\varepsilon = \mu$. Provided that this function is not too rapidly varying in this neighborhood, just a few terms should be needed. Since the derivative $f'(\varepsilon)$ is symmetric around

the value of the chemical potential μ, the first nonvanishing contribution to $I(T, \mu)$, in addition to $G(\mu)$, is of second order in the Taylor expansion of G:

$$G(\varepsilon) = G(\mu) + (\varepsilon - \mu) \, G'(\mu) + \tfrac{1}{2} (\varepsilon - \mu)^2 \, G''(\mu). \quad (16)$$

At second order, one obtains

$$I(T, \mu) = G(\mu) - \frac{1}{2} G''(\mu) \int_{-\infty}^{\infty} (\varepsilon - \mu)^2 f'(\varepsilon) \, d\varepsilon. \quad (17)$$

To evaluate the remaining integral, the following change of variable is done

$$z = \beta(\varepsilon - \mu), \quad (18)$$

leading to

$$I(T, \mu) = G(\mu) + a_1 \, G''(\mu) \, (k_B T)^2, \quad (19)$$

with

$$a_1 = \frac{1}{2} \int_{-\infty}^{\infty} z^2 \frac{e^z}{(1 + e^z)^2} \, dz. \quad (20)$$

Using the Taylor expansion at all orders leads to the Sommerfeld expansion [26,27]:

$$\int_{-\infty}^{\infty} g(\varepsilon) f(\varepsilon) \, d\varepsilon$$
$$= \int_{-\infty}^{\mu} g(\varepsilon) \, d\varepsilon + \sum_{n=1}^{\infty} a_n \, (k_B T)^{2n} \left. \frac{d^{2n-1} g}{d\varepsilon^{2n-1}} \right|_{\mu}, \quad (21)$$

where a_n is related to the zeta function by

$$a_n = 2(1 - 2^{1-2n}) \, \zeta(2n). \quad (22)$$

A complete expansion in θ needs to include the expansion of the chemical potential μ, too. To this end, the DOS $n(\varepsilon)$ is introduced such that

$$\frac{N_e}{V} = \int_{-\infty}^{\infty} n(\varepsilon) f(\varepsilon) \, d\varepsilon, \quad (23)$$

where N_e is the total number of electrons in a volume V. One can then show that, at second order in θ:

$$\mu = \varepsilon_F \left[1 - \frac{\pi^2}{6} \frac{\varepsilon_F n'(\varepsilon_F)}{n(\varepsilon_F)} \theta^2 \right], \quad (24)$$

provided that the DOS $n(\varepsilon)$ does not vary from 0 K to T. As a consequence, μ can be replaced by ε_F in every term of second order in θ. In the same spirit, one gets

$$\int_{-\infty}^{\mu} g(\varepsilon) \, d\varepsilon = \int_{-\infty}^{\varepsilon_F} g(\varepsilon) \, d\varepsilon - \frac{\pi^2}{6} \frac{\varepsilon_F n'(\varepsilon_F)}{n(\varepsilon_F)} g(\varepsilon_F) \theta^2. \quad (25)$$

We sum up with the expression of the Sommerfeld expansion at second order in θ:

$$\int_{-\infty}^{\infty} g(\varepsilon) f(\varepsilon) \, d\varepsilon$$
$$= \int_{-\infty}^{\varepsilon_F} g(\varepsilon) \, d\varepsilon + \frac{\pi^2}{6} \varepsilon_F^2 \left[g'(\varepsilon_F) - \frac{n'(\varepsilon_F)}{n(\varepsilon_F)} g(\varepsilon_F) \right] \theta^2. \quad (26)$$

As in the case of Eq. (24), the function $g(\varepsilon)$ is assumed to stay unchanged from 0 K to T. Otherwise, there is an implicit dependence on temperature in every term involving g or its derivative.

C. Sommerfeld-like expansion of entropy

A Sommerfeld-like expansion of the electronic entropy, as given by Eq. (8), can be performed using the function $s(\varepsilon)$ in lieu of the FD derivative $f'(\varepsilon)$. Provided that the DOS $n(\varepsilon)$ is not too rapidly varying in the neighborhood of the chemical potential, it can be Taylor-expanded within the integral. At second order, one gets

$$n(\varepsilon) = n(\mu) + (\varepsilon - \mu) \, n'(\mu) + \tfrac{1}{2}(\varepsilon - \mu)^2 \, n''(\mu). \quad (27)$$

Again, the term of order 1 does not contribute since the function $s(\varepsilon)$ is symmetric about the value of the chemical potential μ:

$$\frac{S}{V k_B} = -n(\mu) \int_{-\infty}^{+\infty} s(\varepsilon) \, d\varepsilon$$
$$- \frac{1}{2} n''(\mu) \int_{-\infty}^{+\infty} (\varepsilon - \mu)^2 \, s(\varepsilon) \, d\varepsilon. \quad (28)$$

The integrals are evaluated using the same change of variable as before:

$$z = \beta(\varepsilon - \mu), \quad (29)$$

leading to

$$\frac{S}{V k_B} = b_1 \, n(\mu) \, k_B T + b_3 \, n''(\mu) \, (k_B T)^3, \quad (30)$$

with (see Appendix C)

$$b_1 = 2 \int_{-\infty}^{+\infty} \frac{\ln(1 + e^z)}{1 + e^z} \, dz = \frac{\pi^2}{3}, \quad (31)$$

and

$$b_3 = \int_{-\infty}^{+\infty} z^2 \frac{\ln(1 + e^z)}{1 + e^z} \, dz = \frac{7\pi^4}{90}. \quad (32)$$

More generally, for the $(k_B T)^{2n+1}$ term in the expansion, one is faced with the evaluation of the integral

$$\int_{-\infty}^{+\infty} z^{2n} \frac{\ln(1 + e^z)}{1 + e^z} \, dz. \quad (33)$$

As before, to account for the temperature dependence of the chemical potential μ, we use Eq. (24) to get a Sommerfeld-like expansion at third order:

$$\frac{S}{V k_B} = b_1 \, \varepsilon_F \, n(\varepsilon_F) \, \theta$$
$$+ \varepsilon_F^3 \left(\frac{\pi^2}{6} b_1 \frac{[n'(\varepsilon_F)]^2}{n(\varepsilon_F)} + b_3 \, n''(\varepsilon_F) \right) \theta^3. \quad (34)$$

At first order, this expansion provides a great simplification since the temperature dependence of entropy is an explicit linear factor. The coefficient of the temperature is a function of density only. Unfortunately, this coefficient involves the DOS, which is the main ingredient of the exact calculation of entropy according to Eq. (8). From a practical point of view, it is, therefore, only the linear temperature dependence that needs be checked as a useful approximation. We shall investigate in the following results the domain of validity of this Sommerfeld expansion. One can conjecture that it breaks down when the DOS $n(\varepsilon)$ does not vary smoothly in the vicinity of the chemical potential value μ. When the AA model

predicts that the atom is neutral at sufficiently low density and temperature, there are only bound states in the DOS with Dirac distribution according to Eq. (7). In Appendix B, a discussion is provided about the AA predictions in this limit of a neutral atomic gas. In other circumstances, as the density increases at low temperature, pressure ionization can occur that leads to resonances in the DOS, and one can wonder whether this impedes the validity of the Sommerfeld expansion.

D. FEG

Here, we describe a much simpler model than the AA one. This simple solution to our problem is the FEG model. It has met with great success in solid state physics in its beginning. Sommerfeld [26] proposed this model to improve Drude's model of conductivity [27]. He assumed that the interaction between the ions and the valence electrons can be neglected, the ions being only responsible for the charge neutrality in the metal. He further assumed that the interactions between electrons can be ignored as a result of screening effects. More importantly, he stressed that the Pauli exclusion principle requires that each quantum state of the system can only be occupied by a single electron, this restriction of available electron states being taken care of by FD statistics.

For our purpose, we shall only need the nonrelativistic version of this model. The relativistic effects are only important for bound states at low temperature. The relativistic formulation is more involved and can be found in Faussurier's paper [46].

In the FEG model, the Fermi energy depends on the electron density n_e, which is uniform in the model, through

$$\varepsilon_F = \tfrac{1}{2} (3\pi^2 n_e)^{2/3}. \quad (35)$$

Defining a mean ionization Z^* by $n_e = Z^* n_i = Z^*/V$, one can see that $\varepsilon_F \propto (Z^* \rho)^{2/3}$ in this model. The DOS $n(\varepsilon)$ reads

$$n(\varepsilon) = \frac{3}{2} \frac{n_e}{\varepsilon_F} \sqrt{\frac{\varepsilon}{\varepsilon_F}} = \frac{1}{\pi^2} \sqrt{2\varepsilon}, \quad (36)$$

leading to the Sommerfeld expansion at first order in $\theta = k_B T / \varepsilon_F$:

$$S = \tfrac{3}{2} k_B b_1 Z^* \theta. \quad (37)$$

To sum up, the entropy per atom S is proportional to $(Z^*)^{1/3} \rho^{-2/3} T$ at first order in the Sommerfeld expansion within the FEG model.

III. RESULTS

We have adapted to INFERNO-like modeling an AA code developed by Bruneau [47] to study the model proposed by Rozsnyai [32], where the discrete bound states are broadened into canonical bands, and recently improved by Massacrier et al. [33] and Callow et al. [34], where the free states are computed quantum-mechanically instead of treated within the semiclassical TF approximation used by Rozsnyai. Bruneau's code differs from these recent works by the use of the Dirac equation instead of the Schrödinger equation. We named this INFERNO-like adaptation of Bruneau's code NIRVANA.

Using NIRVANA, we computed the entropy of hydrogen (H, $Z = 1$, $A = 1.00784$, belonging to the s blocks of the

periodic table), aluminum (Al, $Z = 13$, $A = 26.98$, belonging to the p blocks), iron (Fe, $Z = 26$, $A = 55.845$, belonging to the d blocks), and cerium (Ce, $Z = 58$, $A = 140.12$, belonging to the f blocks). The thermodynamic conditions of temperature T and density ρ cover the range from 0.01 to 10 eV and 10^{-4} to 10^4 g cm^{-3}. The T-ρ grid is logarithmic with 6 points per decade in T and ρ, at 1, 1.47, 2.15, 3.16, 4.64, and 6.81. For each element, two figures show the two facets provided by isochores and isotherms. Since the entropy is an increasing function of temperature, the isotherms are in decreasing order of temperature from top to bottom. As for the isochores, they are in increasing order of density from top to bottom since the entropy is a decreasing function of the density. We used the KS XC functional [41]. The sensitivity of the results to the choice of XC functional is investigated in Sec. IV C.

A. Hydrogen

With its simple electronic structure composed of only one electron per atom, hydrogen already exhibits the main features that are met for other elements. It is clear from Fig. 2 that there are two regimes: At low enough density, the AA model predicts that the atom is neutral with only bound states, whereas at high density, there is a continuum of free states sitting on a fully occupied electronic configuration, only the nucleus in the hydrogen case. The transition between both regimes is rather abrupt, here at around 0.1–0.2 g cm^{-3}, with a WS radius of the confinement sphere $r_{ws} = 2$–$3\,a_0$, where a_0 is the Bohr radius. This is reminiscent of Mott's prediction of metal-insulator transition when the number of free electrons within a sphere of radius equal to a_0 vanishes [48]. Before this transition, there is a slight increase of the entropy values with increasing density (see the bottom panel of Fig. 2). This nonphysical behavior is to be attributed to the possible lack of thermodynamic consistency discussed in Sec. II A.

The low-density regime can be described as composed of neutral atoms until the temperature reaches values higher than ~ 0.5 eV. The entropy of the neutral atom is equal to 1.39 k_B per atom, in accordance with the analysis presented in Appendix B applied to hydrogen with only one electron in the $1s_{1/2}$ bound state. For temperature > 0.5 eV, there is a thermal electronic contribution to the EOS, which increases with the ionization triggered by the rise of temperature. At these high temperatures, the entropy along isochores does not depend on temperature linearly, and the Sommerfeld expansion is not valid.

In the high-density regime, one observes the linear dependence of entropy with temperature predicted by the Sommerfeld expansion (see the top panel of Fig. 2). The coefficient of the temperature in the expansion depends on density as a power law around $\rho^{-2/3}$ (see the bottom panel of Fig. 2). These dependencies on temperature and density suggest that compressed hydrogen behaves as a FEG (see Sec. II D). We shall see in Sec. IV C that this is only approximate. Interestingly, the density power law does not apply to the intermediate density regime between 0.2 and 0.4 g cm^{-3}, which presents a weaker slope due to the dissolution of the resonant feature, associated with the ionized $1s_{1/2}$ state, in the DOS of free states.
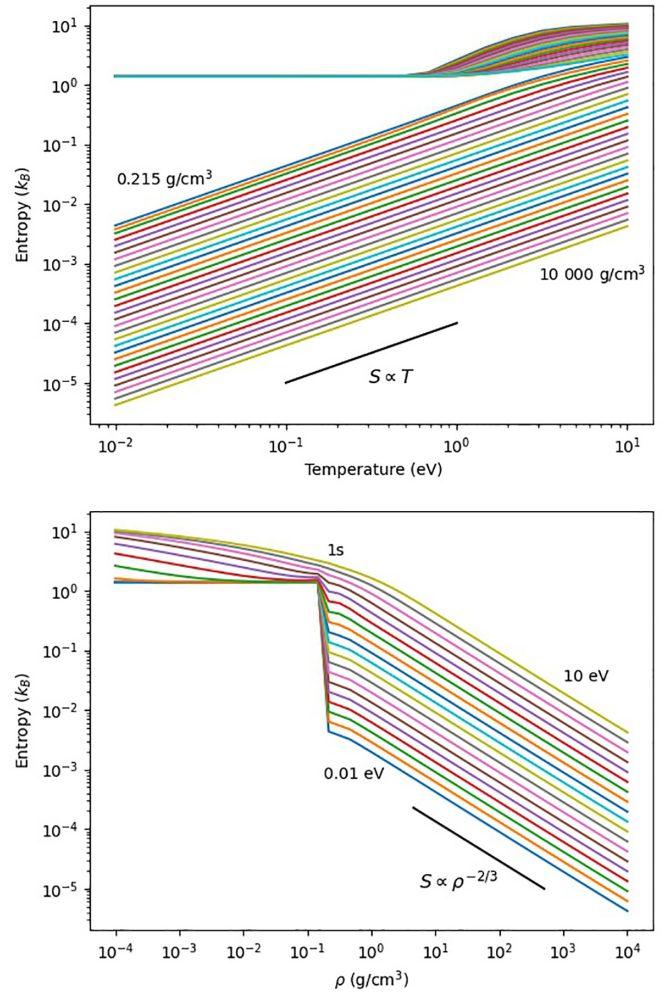

FIG. 2. Isochores (top) and isotherms (bottom) of electronic entropy per atom obtained for hydrogen using the INFERNO-like model implemented in the NIRVANA code. There are 6 points per decade in T and ρ, at 1, 1.47, 2.15, 3.16, 4.64, and 6.81. The range in density of pressure ionization of the $1s$ state is indicated with its label in the bottom panel.

B. Aluminum

The results for aluminum are presented in Fig. 3. For one of the isochores at $\rho = 31.6$ g cm^{-3}, characteristic of the pressure ionization of the $2p_{1/2}$ and $2p_{3/2}$ states, the NIRVANA code did not reach convergence. This engages six electrons which transit from the bound states to associated resonances from one iteration to the following, during the self-consistent-field search for convergence. The numerics are toughly stressed since the chemical potential μ varies strongly according to the configurations with bound states or resonances, and a strong requirement of discretization around μ is required. We did not pursue the numerical effort to resolve this issue since there exist ways to circumvent it by a broadening of the discrete bound states using canonical bands [32–34] or, more rigorously, albeit involved, using the Green's function approach, extending the eigenvalue problem to the complex plane, as introduced by Starrett [49,50]. Instead, we interpolated the results of the nearest converged isochores at 27.5 and 33.5 g cm^{-3}.
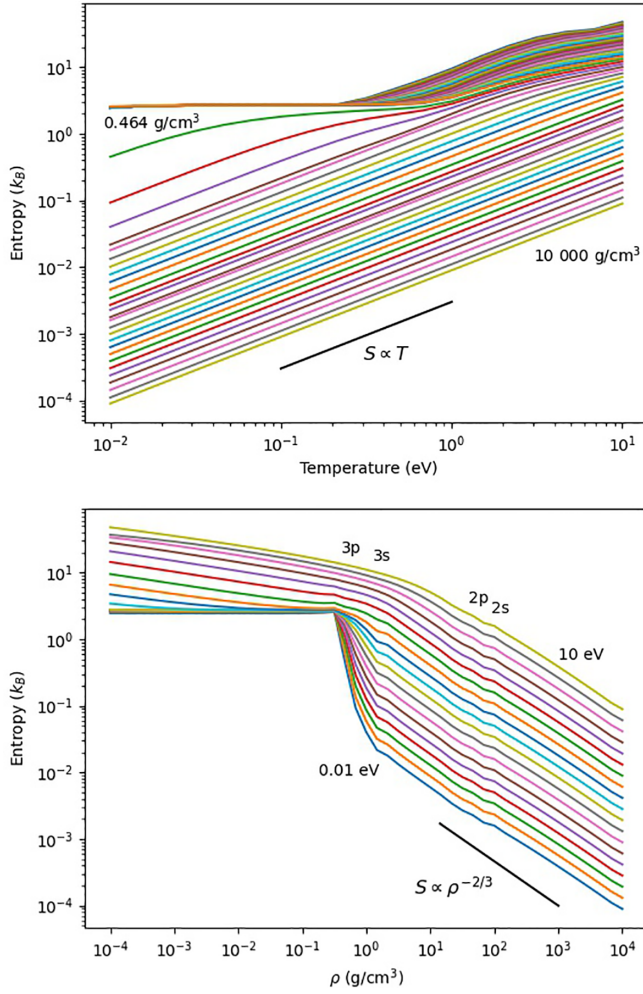
FIG. 3. Isochores (top) and isotherms (bottom) of electronic entropy per atom obtained for aluminum using the INFERNO-like model implemented in the NIRVANA code. There are 6 points per decade in T and ρ, at 1, 1.47, 2.15, 3.16, 4.64, and 6.81. The range in density of pressure ionization of each bound state is indicated with the state label in the bottom panel.
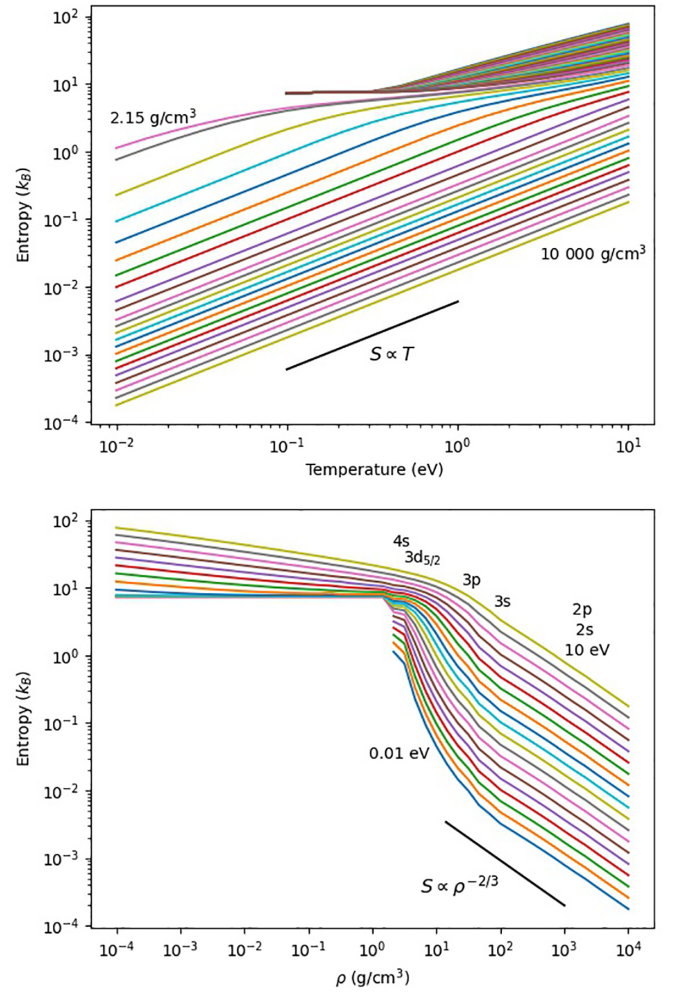
FIG. 4. Isochores (top) and isotherms (bottom) of electronic entropy per atom obtained for iron using the INFERNO-like model implemented in the NIRVANA code. There are 6 points per decade in T and ρ, at 1, 1.47, 2.15, 3.16, 4.64, and 6.81. The range in density of pressure ionization of each bound state is indicated with the state label in the bottom panel.

The transition from the low-density regime to the high-density one occurs between 0.3 and 0.7 g cm^{-3}, corresponding to WS radii between 5 and 6 a_0.

The low-density regime can be described as composed of neutral atoms with the following configuration: [Ne] $3s_{1/2}^2\,3p_{1/2}^{0.36}\,3p_{3/2}^{0.64}$. In this case, the level $3p_{1/2}$ and $3p_{3/2}$ are close in energy, -0.0719 and -0.0713 a.u., respectively, and their FD factor is almost the same, $\sim\frac{1}{6}$. Assuming a nonrelativistic configuration with only one electron on the $3p$ shell, the analysis presented in Appendix B predicts a value of the entropy per atom of 2.7 k_B in accordance with the result of NIRVANA. For temperature >0.2 eV, there is a thermal electronic contribution to the EOS, which does not depend on temperature linearly as in the Sommerfeld expansion.

In the high-density regime, the entropy depends linearly on temperature as predicted by the Sommerfeld expansion (see the top panel of Fig. 3). The function that multiplies the temperature in this expansion seems to depend on both density and ionization. In the bottom panel of Fig. 3, each isotherm

exhibits a plateau in the same small density range whenever pressure ionization occurs. In these plateaus, the entropy is more or less constant as a result of the progressive dissolution of the associated resonance. In between these plateaus, the entropy follows the power law around $\rho^{-2/3}$ of the FEG at a level that seems to adjust to the new ionization as suggested by the FEG model [see Eq. (37) in Sec. II D]. Here, the AA model predicts shell effects that are not accounted for by the FEG model. Elucidating whether these shell effects are realistic or artifacts deserves further investigation.

C. Iron

The results for iron are presented in Fig. 4. In this case, the AA model, as implemented in the NIRVANA code, is faced with an issue related to the convergence of the neutral atom configuration at low temperature. At a temperature of 0.1 eV, the converged configuration is [Ar] $3d_{3/2}^{3.15}\,3d_{5/2}^{3.54}\,4s_{1/2}^{1.31}$ with a value of the entropy of 7.41 k_B. The three last partially occupied levels are located at close energies of -0.1452, -0.1400,

and −0.1415 a.u. A fictitious degenerate level, assembling these three levels, of degeneracy 12 with occupancy 7, leads to a value of the entropy of 8.15 k_B according to the analysis of Appendix B. At temperatures <0.1 eV, the spread around the chemical potential in the FD distribution lessens, and the three levels are much more in competition. Each preferred level leads to a different screening of the nucleus charge favoring another level, and so on. As discussed in Appendix B, the best method to determine the fundamental state of an isolated atom requires a multiconfiguration-interaction calculation that cannot compete with the DFT formulation. Thus, we left aside the corresponding parts of the isochores, namely, for densities <1.47 g cm^{-3} and temperatures <0.1 eV.

The transition from the low-density regime to the high-density one occurs between 1.5 and 2.3 g cm^{-3}, corresponding to WS radii between 4.0 and 4.6 a_0.

As for the other elements, ionization shows up in the low-density regime above a temperature of ∼0.3 eV. It produces a thermal electronic contribution to the EOS, which again does not depend on temperature linearly as in the Sommerfeld expansion.

In the high-density regime, the entropy depends linearly on temperature, as predicted by the Sommerfeld expansion (see the top panel of Fig. 4). In the bottom panel of Fig. 4, the values of the entropy decrease with increasing density with a higher slope than the power law of $\rho^{-2/3}$ characteristic of the FEG, along each isotherm. It is only for density >100 g cm^{-3} that the FEG behavior is recovered.

D. Cerium

The results for cerium are presented in Fig. 5. In this case, the AA model, as implemented in the NIRVANA code, is faced with both issues met by aluminum and iron. As with iron, the convergence of the neutral atom configuration at low temperature is only reached at a temperature of 0.1 eV. Therefore, for the same reasons, we left aside the data for densities <3.16 g cm^{-3} and 0.1 eV. As with aluminum, one of the isochores at $\rho = 1470$ g cm^{-3} presents convergence issues related here to the pressure ionization of the $3d_{3/2}$ bound state. Thus, we interpolated the results of the nearest isochores at 1400 and 1600 g cm^{-3}.

The transition from the low-density regime to the high-density one occurs between 2 and 3 g cm^{-3}, corresponding to WS radii between 5 and 6 a_0.

The DFT approach used in the AA model predicts a value of the entropy for the neutral atom at 0.1 eV of 5.71 k_B per atom. At a temperature of 0.1 eV, the converged configuration is [Xe] $4f_{5/2}^{1.36}\, 4f_{7/2}^{0.11}\, 5d_{3/2}^{0.41}\, 5d_{5/2}^{0.12}\, 6s_{1/2}^{2}$. Here, there are four partially occupied levels with close energies of −0.0709, −0.0597, −0.0675, and −0.0613 a.u., respectively. Assembling these four levels into a fictitious level of degeneracy 24 with occupancy 2 leads to a value of the entropy of 6.88 k_B according to the analysis of Appendix B. Ionization shows up in this low-density regime above a temperature of ∼0.2 eV, without a linear dependence in temperature as in the Sommerfeld model.

In the high-density regime, the entropy depends linearly on temperature as predicted by the Sommerfeld expansion (see the top panel of Fig. 5). In the bottom panel of Fig. 5, the
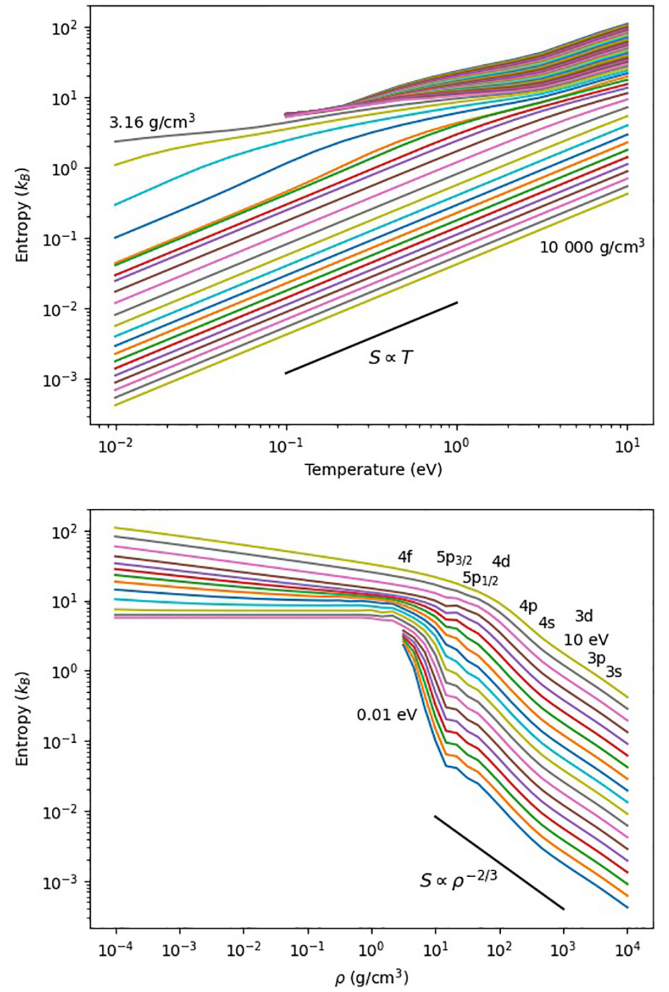

FIG. 5. Isochores (top) and isotherms (bottom) of electronic entropy per atom obtained for cerium using the INFERNO-like model implemented in the NIRVANA code. There are 6 points per decade in T and ρ, at 1, 1.47, 2.15, 3.16, 4.64, and 6.81. The range in density of pressure ionization of each bound state is indicated with the state label in the bottom panel.

values of the entropy decrease with increasing density with a higher slope than the power law around $\rho^{-2/3}$ of the FEG, along each isotherm. It is only for density >250 g cm^{-3} that the FEG behavior is recovered.

IV. ANALYSIS

A. Sommerfeld approximation

As a global exploitation of the results presented in Sec. III, we check the linear dependence on temperature of the electronic entropy in Fig. 6, where each isotherm is divided by the corresponding temperature, for each element. The curves are plotted as functions of the WS radius r_{ws} to get rid of the unnecessary dependence on the molar mass A. Then the entropy is an increasing function of the WS radius. In the considered conditions, the lowest isotherm corresponds to the highest temperature of 10 eV when the entropy is divided by temperature. Respectively, the highest isotherm corresponds to the lowest temperature of 0.01 eV. To easily
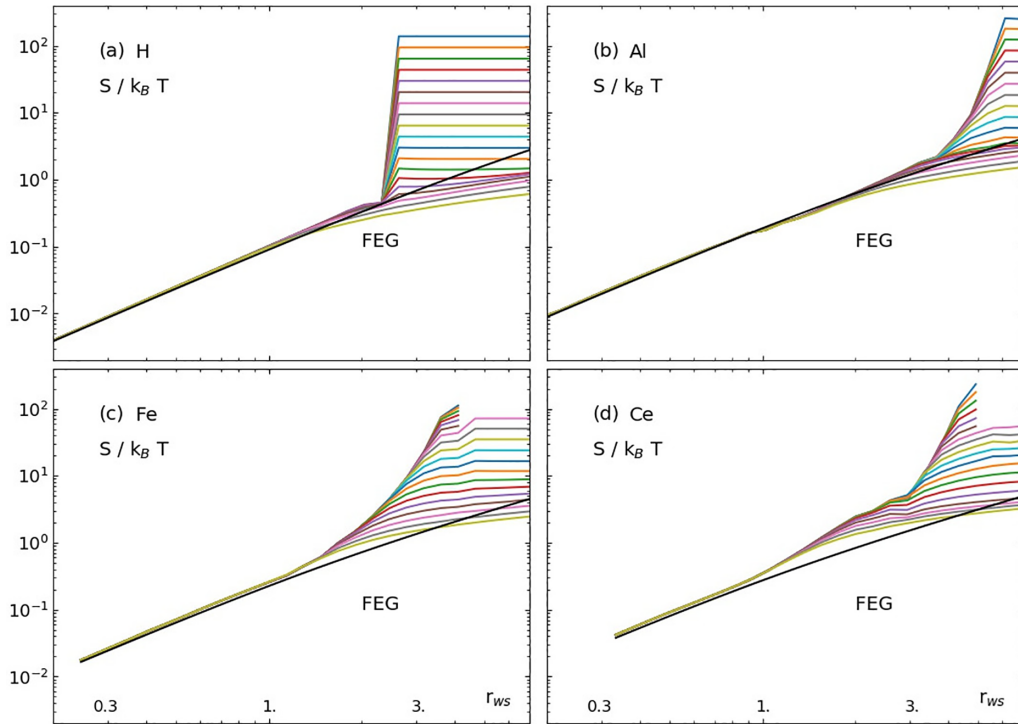
FIG. 6. Isotherms of electronic entropy S in k_B per atom divided by T in electronvolts as a function of r_{ws} obtained for (a) hydrogen, (b) aluminum, (c) iron, and (d) cerium, using the INFERNO-like model implemented in the NIRVANA code. Comparison is also presented with the free electron gas (FEG) using More's fit of the Thomas-Fermi ionization (black lines).

compare the levels and slopes of the isotherms, we keep the same frame for all panels, with the same ranges of WS radii and electronic entropy values. We added the prediction of the FEG model using the TF ionization, given by More's fit [25]. We checked that the ionization given by NIRVANA does not change these predictions. This is due to the weak dependence on Z^* of the FEG model.

The linear dependence on temperature of Sommerfeld's model is observed at low temperatures in the high-density regime, for values of the WS radii $r_{ws} < 2$–6 Bohr radius (a_0) according to where each element transits to a neutral system. The FEG model with TF ionization does a good job up to values of $r_{ws} \sim 1$, in a highly compressed regime. For higher values of r_{ws}, lower densities, NIRVANA results depart from the FEG predictions more or less depending on the element. In this range of r_{ws} values, above $r_{ws} = 1$, the computed isotherms leave Sommerfeld's prediction progressively, the highest temperatures at a lower r_{ws} value than the lowest temperatures. As a metric for the temperature domain of validity of the Sommerfeld expansion, we propose using the degeneracy ratio $\theta = k_B T / \varepsilon_F$ using the TF ionization for the evaluation of the Fermi energy ε_F, as in the FEG model. A visual inspection of Fig. 6 allows one to keep track of the values of r_{ws} where each isotherm moves away from the common line by 10% in entropy value. This indicates that the linearity of the electronic entropy with temperature ceases above $\theta = 0.4$ for hydrogen, 0.3 for aluminum, and 0.05 for iron and cerium. Based on these results, we propose adopting a conservative limit of $\theta = 0.05$ for all elements. Needless to say, this prescription requires further investigation. Together with the limit in WS radius r_{ws} of the metal-insulator transi-

tion, the limit in degeneracy ratio θ allows one to study the Sommerfeld expansion of the electronic entropy for a given chemical element from only one isotherm at sufficiently low temperature. We pursue this line of investigation in Sec. IV B, where trends with the atomic number Z are studied.

B. Z trends

The preceding analysis of Sec. IV A suggests determining the density-dependent coefficient of temperature in the Sommerfeld expansion for all chemical elements using just one isotherm at sufficiently low temperature. To set up this temperature, we decided to look for a value T which leads to degeneracy parameter θ less than the limit of 0.05 in the whole range of WS radius values r_{ws} of the high-density regime, which is limited from above by the metal-insulator transition. Since $\varepsilon_F \propto (Z^*)^{2/3} / r_{ws}^2$, the highest value of θ is obtained from the lowest value of ε_F, using $Z^* = 1$ and the highest value of r_{ws} for the metal-insulator transition. We shall see that this maximum r_{ws} value is ~ 8. (see Fig. 7) leading to a value of the Fermi energy of $\varepsilon_F \sim 0.8$ eV. The limit temperature corresponding to $\theta = 0.05$ is then $T = 0.04$ eV. We adopted $T = 0.01$ eV as a conservative choice. The corresponding isotherm was computed in the density range from 0.1 to 10^4 g cm^{-3} for the elements of atomic number Z in the range from 1 (hydrogen) to 71 (lutetium).

1. Metal-insulator transitions

We determined the value of the WS radius r_{ws} at the metal-insulator transition by visual inspection for each element. As Fig. 7 shows, there is no trend following the atomic number
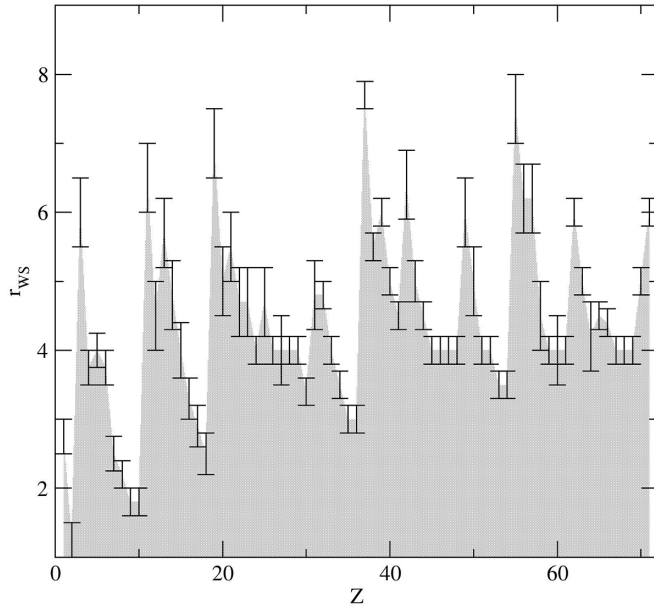
FIG. 7. Wigner-Seitz (WS) radii at the metal-insulator transition in NIRVANA as a function of the atomic number Z.

FIG. 8. Ratios between the electronic entropy S predicted by NIRVANA and the free electron gas (FEG) model at 0.01 eV for elements from $Z = 1$ (hydrogen) to 71 (lutetium) as a function of the Wigner-Seitz (WS) radius. Also plotted is a linear regression in the range of r_{ws} values from 0 to 1.

Z, except for the natural sequence following the periodic table of the elements. Overall, a typical limit of $r_{ws} = 4 a_0$ obtrudes. As we shall see in Sec. IV C, these values of the critical WS radius are highly sensitive to the XC functional used.

2. FEG regimes

We checked the validity domain of the FEG model by computing for each element the ratio between the electronic entropy values computed with NIRVANA and predicted by the FEG model as a function of the WS radius, for the isotherm at 0.01 eV. The results are gathered in Fig. 8. For WS radii $r_{ws} < 1$, the spread among the results is <20% with a tendency for higher electronic entropy than predicted by the FEG model as the value of 1 is reached. An empirical correction of linear form, $c_0 + c_1 r_{ws}$, with $c_0 = 1.023$ and $c_1 = 0.137$, can multiply the FEG formula for the entropy S leading to an accuracy of $\pm 10\%$ in this range. For WS radii $r_{ws} > 1$, we did not observe any trends with the atomic number Z. In this range, accurate results can only be obtained from the AA code. We provide a small database in Supplemental Material [51] to satisfy this need. Finally, although the FEG model does not completely reproduce the AA results at all WS radii, it flattens out the main trend of increase in electronic entropy S as the density ρ decreases or, alternatively, the WS radius r_{ws} increases. Comparing Figs. 6 and 8, the variations of S no longer spread over decades. We shall use this normalization of S by the FEG predictions in Sec. IV C to highlight the sensitivity to XC functionals.

C. Sensitivity to XC

Here, we investigate the sensitivity of the AA predictions of electronic entropy S to the choice of XC functionals used. We compare the choices of the KS [41], Slater [52], and Van Leeuwen [53] functionals, and the choice not to include any
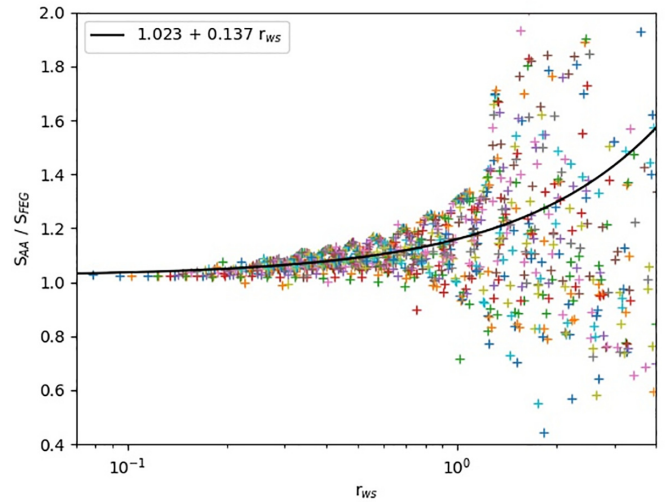
XC contribution. Although this set of functionals is limited, it is sufficient to highlight the main sensitivities. The XC functionals used are exchange-only functionals, neglecting the contribution from correlation. The KS and Slater functionals belong to the family of Xα functionals, with the following exchange potential:

$$V_{X\alpha}(r) = -\frac{3}{2} X_\alpha \left(\frac{3}{\pi}\right)^{1/3} \rho(r)^{1/3}, \tag{38}$$

with $X_\alpha = 1$ for the Slater functional and $X_\alpha = \frac{2}{3}$ for the KS functional. Both functionals use a local density approximation, whereas the Van Leeuwen functional includes corrections from the gradient of density, with a potential given by

$$V_{VL}(r) = -\beta \rho(r)^{1/3} \frac{x^2}{1 + 3\beta x \sinh^{-1}(x)}, \tag{39}$$

with the dimensionless quantity:

$$x = \frac{|\nabla \rho|}{\rho^{4/3}}. \tag{40}$$

In contrast to other nonlocal approximations [5,6], the Van Leeuwen potential was built as an attempt to preserve the asymptotic Coulombic behavior of the exchange potential, leading to a self-interaction correction.

The analysis of the preceding Secs. IV, IV B, and IV B 2, prompts us to restrict the comparison between the results using different XC functionals to just one isotherm at 0.01 eV. It also demonstrates that the ratio between the values of electronic entropy S predicted by the AA and FEG models as a function of the WS radius r_{ws} is most appropriate to highlight any discrepancies. In Fig. 9, this ratio is plotted as a function of the WS radius r_{ws} for the preceding choices of XC functionals, at a constant temperature of 0.01 eV, for hydrogen in panel (a), aluminum in panel (b), iron in panel (c),
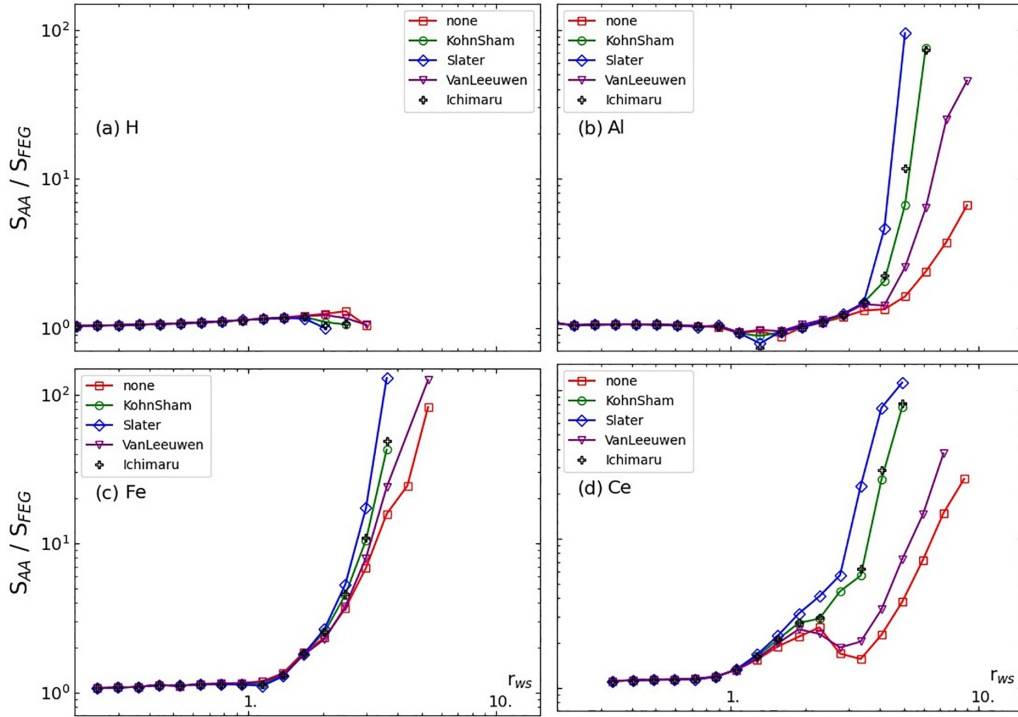
FIG. 9. Sensitivity to the exchange-correlation (XC) functional of the ratio between the electronic entropy S_{AA} predicted by NIRVANA and S_{FEG} predicted by the free electron gas (FEG) model at 0.01 eV as a function of the Wigner-Seitz (WS) radius r_{ws}. Five choices are compared: no XC functional, the Kohn-Sham functional [41], the Slater functional [52], the Van Leeuwen functional [53], and a temperature-dependent XC functional (Ichimaru [54]). Hydrogen is depicted in panel (a), aluminum in panel (b), iron in panel (c), and cerium in panel (d). Each curve is stopped at the WS radius where a metal-insulator transition occurs.

and cerium in panel (d). As expected for a weakly correlated electron system, the sensitivity to the XC choice is weak at high density, for WS radii <1–2. For higher WS radii, at moderate density, discrepancies among the different XC choices show up. They are responsible for different values of the WS radius r_{ws} for the metal-insulator transition and different transitory behaviors between $r_{ws} \sim 2$ and this critical WS radius.

We end this sensitivity study by addressing the influence of a temperature-dependent XC functional, namely, the one proposed by Ichimaru *et al.* [54]. As discussed in Sec. II A, this gives rises to a XC contribution to the entropy S_{xc}, which is negligible in the validity domain of the

Sommerfeld approximation, delineated by the degeneracy parameter $\theta < 0.05$. In Fig. 9, the results obtained with the Ichimaru functional closely follow the KS ones since the latter functional is the low-temperature limit of the exchange part of the chosen temperature-dependent XC functional. To monitor the behavior of the electronic entropy computed with different XC functionals as a function of temperature, Table I gathers the values obtained with the exchange-only 0 K KS functional, the XC temperature-dependent Ichimaru functional, and the choice not to account for XC effects (none). At the low temperatures of 0.01 and 0.1 eV, in the validity domain of the Sommerfeld approximation ($\theta < 0.05$), this comparison highlights the strong influence of exchange and to a lesser extent of correlation (0.01 k_B/atom). The effect of the temperature dependence of the Ichimaru functional seems to appear as a small correction between 1 and 10 eV.

V. CONCLUSIONS

The main purpose of this paper was to contribute to the modeling of the electron-thermal part of the EOS in the low-temperature regime, characteristic of solids and liquid metals. Among the different approaches used in the models for the multiphase EOS, the AA is considered the method providing the best compromise between accuracy, robustness, and computation time to obtain the electron-thermal contribution. Our analysis through the prism of Sommerfeld expansion lays a simplification, which can afford to avoid the pitfalls related to pressure ionization and the often associated discontinuities

TABLE I. For cerium at $\rho = 5.857$ g/cm^3 ($r_{ws} = 4$), comparison as a function of temperature T in electronvolts between electronic entropy in k_B per atom computed with different XC functionals: Kohn-Sham, an exchange-only functional; Ichimaru, a temperature-dependent XC functional; and the choice not to account for XC, none. The degeneracy parameter $\theta = k_B T / \varepsilon_F$.

T (eV)	θ	S_{none} (k_B/atom)	$S_{Kohn-Sham}$ (k_B/atom)	$S_{Ichimaru}$ (k_B/atom)
0.01	0.0015	0.0504	0.503	0.590
0.1	0.015	0.502	2.87	3.03
1	0.146	4.51	7.73	7.87
10	1.18	24.8	24.4	24.3

in thermodynamic variables. It also provides orders of magnitude of sensitivity of the electronic entropy to modeling options.

Using an AA framework like the INFERNO model, we probed the validity of the Sommerfeld approximation to the electronic entropy at low temperature. We performed a thorough analysis of four different elements belonging to the s, p, d, and f blocks of the periodic table, namely, hydrogen, aluminium, iron, and cerium. This allowed us to delineate the validity domain of Sommerfeld approximation in temperature and density. The dimensionless ratio $\theta = k_B T / \varepsilon_F$ reducing the temperature to the Fermi energy must be less than ~ 0.05 to preserve a linear dependence of the entropy on temperature. In this range of temperature, the coefficient of temperature is a function of density, which can be investigated using just one isotherm at sufficiently low temperature. This allowed us to extend the analysis to a broader set of atomic numbers Z. The only trend with Z is that the FEG model is within 10% of the AA prediction at very high density, for WS radius $r_{ws} < 1$, provided that a linear scaling in r_{ws} is adopted with a 14% increase at $r_{ws} = 1$.

At contrast with the semiclassical TF AA model, the quantum-mechanical version includes shell effects but, most importantly, predicts that a metal-insulator transition occurs, although it is often missing from the multiphase EOS. The study of various elements with different atomic number Z evidenced that a metal-insulator transition is predicted by the quantum-statistical AA model. It occurs at different r_{ws} values according to the element without any other trend than the filling of the periodic table. This transition is also very sensitive to the XC functional used. The study of this transition is an active research field [55–62] that we only touched upon since it is beyond the scope of this paper.

As concerns the best modeling choice for the electron-thermal part of the multiphase EOS, we propose starting from the Sommerfeld expansion of the electronic entropy as a foundation. The Sommerfeld expansion of the electronic entropy involves a density-dependent coefficient of the temperature. Depending on the demand of accuracy for multiphase EOS, this coefficient is only approximately given by a power law in density. It is preferable to use the small database of the Supplemental Material [51]. We also showed that the FEG model is of limited value, restricted to very high densities.

We plan to enrich our study with *ab initio* simulations to compare the electronic entropy values and the underlying DOS with the AA ones. Preliminary results suggest that, although there is good agreement in the fluid phase, the crystalline structure induces noticeable discrepancies, which should hopefully be considered by a rescaling of the AA results from a limited number of simulations.

APPENDIX A: ENTROPY ROUTE TO THERMAL EOS

Gibbs provided the following relation from the first principle of thermodynamics:

$$dU = T\,dS - P\,dV + \mu\,dN. \qquad (A1)$$

It expresses the energy conservation in systems in thermodynamic equilibrium where one can define the temperature T, the pressure P, and the chemical potential μ. The variation of

internal energy U is connected to the variations of entropy S, volume V, and number of particles N. In the canonical ensemble, it is the free energy $A(T, V, N)$ that represents the thermodynamic potential through the following Legendre transform:

$$A = U - TS, \qquad (A2)$$

leading to

$$dA = -S\,dT - P\,dV + \mu\,dN. \qquad (A3)$$

At constant volume V_0 and number of particles N_0, the thermal free energy $\Delta A(T, V_0, N_0) = A(T, V_0, N_0) - A(0, V_0, N_0)$ reads

$$\Delta A(T, V_0, N_0) = -\int_0^T S(\tau, V_0, N_0)\,d\tau, \qquad (A4)$$

and at the same time,

$$\Delta A(T, V_0, N_0) = \Delta U(T, V_0, N_0) - T S(T, V_0, N_0), \qquad (A5)$$

since $S(0, V_0, N_0) = 0$ according to the third law of thermodynamics (Nernst theorem). The thermal internal energy $\Delta U(T, V_0, N_0) = U(T, V_0, N_0) - U(0, V_0, N_0)$ is then given as a functional of the entropy by

$$\Delta U(T, V_0, N_0) = -\int_0^T S(\tau, V_0, N_0)\,d\tau + T S(T, V_0, N_0). \qquad (A6)$$

The thermal pressure $\Delta P(T, V_0, N_0) = P(T, V_0, N_0) - P(0, V_0, N_0)$ involves a differentiation of the free energy, which translates into

$$\Delta P(T, V_0, N_0) = \int_0^T \left. \frac{\partial S(\tau, V_0, N_0)}{\partial V_0} \right|_{\tau, N_0} d\tau. \qquad (A7)$$

APPENDIX B: NEUTRAL ATOM GAS

The low-density and low-temperature regime can be described as composed of neutral atoms. In these conditions, there is no reason to add an electronic contribution to the EOS. Here, we comment on the fact that the entropy value obtained within the AA framework for the neutral atom does not vanish as expected.

To find the fundamental state of an isolated atom requires a multiconfiguration computation where all degeneracies are reduced using configuration interaction to get the ultimate term representing the lowest possible state in energy of the atom. This calculation leaves no room for fluctuations, and the value of the entropy should vanish. This is also in line with the absence of any electronic contribution to the EOS. The finite temperature version of DFT cannot compete with such a computation and only predicts an average configuration with possibly partially occupied shells that may lead to nonvanishing values of the entropy.

Within the AA model, when the density and the temperature are so low as to describe a system of neutral atoms, without free states, Eq. (8) reduces to

$$S = -k_B \sum_{s\,\text{bound}} [f_s \ln f_s + (1 - f_s) \ln(1 - f_s)]\, X_s, \qquad (B1)$$

where

$$X_s = 2|\kappa_s| = 2j_s + 1, \tag{B2}$$

since at sufficiently low density, the WS radius is so large that the bound wave functions are completely included in the confinement volume and normalized within it:

$$\int_0^{r_{\mathrm{ws}}} \left[F_s^2(r) + G_s^2(r)\right] dr = 1. \tag{B3}$$

The remaining unknown is the chemical potential μ since

$$f_s = \frac{1}{1 + \exp\left[\beta(\varepsilon_s - \mu)\right]}. \tag{B4}$$

It is given by Eq. (10), which reads without free states as

$$Z = \sum_{s\,\mathrm{bound}} f_s X_s = \sum_{s\,\mathrm{bound}} \frac{2j_s + 1}{1 + \exp\left[\beta(\varepsilon_s - \mu)\right]}. \tag{B5}$$

We also know that, at vanishing temperature, all the levels are fully occupied, from the lowest strongly bound one up to the highest weakly bound one, until the number of available electrons is exhausted. The Fermi energy ε_F is then the energy of the last occupied state. Starting from this picture, we can figure out how the levels are occupied at low temperature. All the lowest levels that can be fulfilled within the limit of Z electrons are occupied. The remaining n_0 electrons partially occupy the next level of degeneracy $X_0 = g_0$. Then Eqs. (B1) and (B5) reduce to

$$S = -k_B[f_0 \ln f_0 + (1 - f_0) \ln(1 - f_0)] g_0, \tag{B6}$$

and

$$n_0 = f_0 g_0 = \frac{g_0}{1 + \exp\left[\beta(\varepsilon_0 - \mu)\right]}. \tag{B7}$$

The value of the chemical potential μ should be easily obtained unless there is more than one level candidate for the level ε_0 in the course of the iterations of the self-consistent field determination. We shall see that this kind of fluctuation occurs in some cases.

There is a situation where the preceding reasoning cannot determine a value for the chemical potential μ. It is when all the levels are fully occupied and there is no more electrons to distribute. In this case, the entropy S vanishes, and the chemical potential μ is undetermined.

APPENDIX C: PROOF OF THE VALUES OF COEFFICIENTS b_1 AND b_3

Below, we provide a proof of the expressions of coefficients b_1 and b_3 defined respectively in Eqs. (31) and (32).

1. Coefficient b_1

We must calculate the integral:

$$b_1 = \int_{-\infty}^{+\infty} \frac{\ln(1 + e^z)}{1 + e^z} dz. \tag{C1}$$

Let us start with the change of variables $u = e^z$, yielding

$$b_1 = \int_0^\infty \frac{\ln(1 + u)}{u(1 + u)} du. \tag{C2}$$

Let us now make the change of variable: $u = t/(1 - t)$. One has $t = u/(1 + u)$ and

$$b_1 = -\int_0^1 \frac{\ln(1 - t)}{t} dt = \mathrm{Li}_2(1), \tag{C3}$$

where

$$\mathrm{Li}_s(z) = \sum_{k=1}^\infty \frac{z^k}{k^s} \tag{C4}$$

is the usual polylogarithm (Li_2 is usually referred to as the *dilogarithm*). One has

$$\mathrm{Li}_n(1) = \zeta(n), \tag{C5}$$

where ζ is the Riemann zeta function. Therefore,

$$b_1 = \zeta(2) = \frac{\pi^2}{6}. \tag{C6}$$

2. Coefficient b_3

The determination of b_3 is more cumbersome. We must calculate the integral:

$$b_3 = \int_{-\infty}^{+\infty} z^2 \frac{\ln(1 + e^z)}{1 + e^z} dz. \tag{C7}$$

Making the same successive two changes of variables $u = e^z$ and $t = u/(1 + u)$ as for b_1, one gets

$$b_3 = -\int_0^1 \frac{[\ln(t) - \ln(1 - t)]^2 \ln(1 - t)}{t} dt, \tag{C8}$$

i.e.,

$$b_3 = -\int_0^1 \frac{\ln^2(t) \ln(1 - t)}{t} dt - \int_0^1 \frac{\ln^3(1 - t)}{t} dt$$
$$+ 2\int_0^1 \frac{\ln(t) \ln^2(1 - t)}{t} dt. \tag{C9}$$

Lewin [63] provides the following expression [eq. (7.48) p. 199 and eq. (7.61) p. 202]:

$$\mathrm{Li}_4(x) = \ln(x)\mathrm{Li}_3(x) - \frac{1}{2}\ln^2(x)\mathrm{Li}_2(x)$$
$$- \frac{1}{2}\int_0^x \ln^2(t)\frac{\ln(1 - t)}{t} dt. \tag{C10}$$

From Eq. (C10) one obtains, taking the limit $x \to 1$,

$$\int_0^1 \frac{\ln^2(t) \ln(1 - t)}{1 - t} dt = -2\zeta(4). \tag{C11}$$

Using eq. (7.62) p. 203 of Ref. [63] or integrating further by parts in Eq (C10) leads to

$$\mathrm{Li}_4(x) = \ln(x)\mathrm{Li}_3(x) - \frac{1}{2}\ln^2(x)\mathrm{Li}_2(x)$$
$$- \frac{1}{6}\ln^3(x)\ln(1 - x) - \frac{1}{6}\int_0^x \frac{\ln^3(t)}{1 - t} dt. \tag{C12}$$

Taking the limit $x \to 1$ in the latter equation and using the property that

$$\int_0^1 \frac{\ln^3(t)}{1 - t} dt = \int_0^1 \frac{\ln^3(1 - t)}{t} dt \tag{C13}$$

gives

$$\int_0^x \frac{\ln^3(1-t)}{t}\,dt = -6\zeta(4). \qquad (C14)$$

The last integral in the right-hand side of Eq. (C9) is slightly more complicated. Let us start by differentiating $\ln^2(x)\ln^2(1-x)/2$:

$$\frac{1}{2}\frac{d}{dx}\ln^2(x)\ln^2(1-x) = \frac{\ln(x)}{x}\ln^2(1-x) - \ln^2(x)\frac{\ln(1-x)}{1-x}. \qquad (C15)$$

Hence, integrating the latter expression implies

$$\frac{1}{2}\ln^2(x)\ln^2(1-x)$$
$$= \int_0^x \frac{\ln(t)}{t}\ln^2(1-t)\,dt - \int_0^x \ln^2(t)\frac{\ln(1-t)}{1-t}\,dt. \qquad (C16)$$

Now let us change the variable from x to $-x/(1-x)$ in Eq. (C12):

$$\mathrm{Li}_4\left(\frac{-x}{1-x}\right) = \ln\left(\frac{x}{1-x}\right)\mathrm{Li}_3\left(\frac{-x}{1-x}\right)$$
$$- \frac{1}{2}\ln^2\left(\frac{x}{1-x}\right)\mathrm{Li}_2\left(\frac{-x}{1-x}\right)$$
$$+ \frac{1}{6}\ln^3\left(\frac{x}{1-x}\right)\ln(1-x)$$
$$+ \frac{1}{6}\int_0^x \ln^3\left(\frac{t}{1-t}\right)\frac{dt}{1-t}. \qquad (C17)$$

Expanding the logarithm:

$$\int_0^x \left[\ln^3(t) - 3\ln^2(t)\ln(1-t) + 3\ln(t)\ln^2(1-t)\right.$$
$$\left. - \ln^3(1-t)\right]\frac{dt}{1-t}, \qquad (C18)$$

we notice that, of the four terms of the latter expression, the first and third have already been dealt with. The fourth is elementary, and the second can be evaluated in terms of the others. One finds, after some algebra (see Ref. [63], formula (7.65), p. 204):

$$\frac{1}{2}\int_0^x \ln^2(t)\frac{\ln(1-t)}{1-t}\,dt = -\mathrm{Li}_4\left(-\frac{x}{1-x}\right) - \mathrm{Li}_4(x)$$
$$+ \mathrm{Li}_4(1-x) - \mathrm{Li}_4(1), \qquad (C19)$$

and

$$\int_0^x \ln^2(t)\frac{\ln(1-t)}{1-t}\,dt$$
$$= +2[\ln(1-x)\mathrm{Li}_3(x) - \ln(x)\mathrm{Li}_3(1-x)]$$
$$+ 2\ln(x)\ln(1-x)\mathrm{Li}_2(1-x)$$
$$- \frac{\pi^2}{6}\ln^2(1-x) + \frac{1}{12}\ln^2(1-x)$$
$$\times [6\ln^2(x) + 4\ln(x)\ln(1-x) - \ln^2(1-x)]$$
$$+ 2\mathrm{Li}_3(1)\ln\left(\frac{1}{1-x}\right). \qquad (C20)$$

As mention by Lewin [63], equating Eqs. (C16) and (C20) simplifies through cancellation of most of the terms due to a particular case of the inversion formula:

$$\mathrm{Li}_n(-x) + (-1)^n \mathrm{Li}_n\left(-\frac{1}{x}\right)$$
$$= -\frac{1}{n!}\ln^n(x) + 2\sum_{r=1}^{\lfloor n/2 \rfloor} \frac{\ln^{n-2r}(x)}{(n-2r)!}\mathrm{Li}_{2r}(-1), \qquad (C21)$$

where $\lfloor y \rfloor$ denotes the integer part of y, and one is left with

$$\int_0^1 \frac{\ln t \ln^2(1-t)}{t}\,dt = -\frac{\zeta(4)}{2}. \qquad (C22)$$

It is worth mentioning that an alternative proof of Eq. (C22) was provided by Connon [64]. Inserting Eqs. (C11), (C14), and (C22) into the right-hand side of Eq. (C9) gives the final result:

$$b_3 = -[-2\zeta(4)] - [-6\zeta(4)] + 2\left[-\frac{\zeta(4)}{2}\right]$$
$$= 7\zeta(4) = \frac{7\pi^4}{90}. \qquad (C23)$$

[1] D. C. Wallace, *Statistical Physics of Crystals and Liquids* (World Scientific, Singapore, 2003).

[2] R. P. Drake, *High-Energy-Density Physics: Foundation of Inertial Fusion and Experimental Astrophysics* (Springer, Berlin, 2018).

[3] J. A. Gaffney, S. X. Hu, P. Arnault, A. Becker, L. X. Benedict, T. R. Boehly, P. M. Celliers, D. M. Ceperley, O. Certík, J. Clérouin *et al.*, High Energy Density Phys. **28**, 7 (2018).

[4] V. Fortov, K. Khishchenko, P. Levashov, and I. Lomonosov, Nucl. Instrum. Methods. Phys. Res. A **415**, 604 (1998).

[5] R. O. Jones, Rev. Mod. Phys. **87**, 897 (2015).

[6] H. S. Yu, S. L. Li, and D. G. Truhlar, J. Chem. Phys. **145**, 130901 (2016).

[7] M. Bonitz, T. Dornheim, Z. A. Moldabekov, S. Zhang, P. Hamann, H. Kählert, A. Filinov, K. Ramakrishna, and J. Vorberger, Phys. Plasmas **27**, 042710 (2020).

[8] A. Blanchet, M. Torrent, and J. Clérouin, Phys. Plasmas **27**, 122706 (2020).

[9] P. Arnault and S. Guisset, Phys. Plasmas **29**, 090901 (2022).

[10] T. J. Callow, S. B. Hansen, E. Kraisler, and A. Cangi, Phys. Rev. Res. **4**, 023055 (2022).

[11] E. D. Chisolm, S. D. Crockett, and D. C. Wallace, Phys. Rev. B **68**, 104103 (2003).

[12] D. C. Swift, T. Lockard, R. G. Kraus, L. X. Benedict, P. A. Sterne, M. Bethkenhagen, S. Hamel, and B. I. Bennett, Phys. Rev. E **99**, 063210 (2019).

[13] P. Vinet, J. H. Rose, J. Ferrante, and J. R. Smith, J. Phys.: Condens. Matter **1**, 1941 (1989).

[14] G. I. Kerley, J. Chem. Phys. **73**, 469 (1980).

[15] J. D. Johnson, High Press. Res. **6**, 277 (1991).

[16] D. C. Swift, M. Bethkenhagen, A. A. Correa, T. Lockard, S. Hamel, L. X. Benedict, P. A. Sterne, and B. I. Bennett, Phys. Rev. E **101**, 053201 (2020).

[17] C. Bhattacharya, Comput. Mater. Sci. **82**, 274 (2014).

[18] L. X. Benedict, K. P. Driver, S. Hamel, B. Militzer, T. Qi, A. A. Correa, A. Saul, and E. Schwegler, Phys. Rev. B **89**, 224109 (2014).

[19] L. H. Thomas, Math. Proc. Cambridge Philos. Soc. **23**, 542 (1927).

[20] E. Fermi, Rend. Accad. Naz. Lincei **6**, 602 (1927).

[21] R. P. Feynman, N. Metropolis, and E. Teller, Phys. Rev. **75**, 1561 (1949).

[22] K. R. Cochrane, P. Kalita, J. L. Brown, C. A. McCoy, J. W. Gluth, H. L. Hanshaw, E. Scoglietti, M. D. Knudson, S. P. Rudin, and S. D. Crockett, Phys. Rev. B **105**, 224109 (2022).

[23] C. J. Wu, P. C. Myint, J. E. Pask, C. J. Prisbrey, A. A. Correa, P. Suryanarayana, and J. B. Varley, J. Phys. Chem. A **125**, 1610 (2021).

[24] J. Meyer-ter-Vehn and W. Zittel, Phys. Rev. B **37**, 8674 (1988).

[25] R. M. More, Adv. At. Mol. Phys. **21**, 305 (1985).

[26] A. Sommerfeld, Z. Phys. **47**, 1 (1928).

[27] N. W. Ashcroft and N. D. Mermin, *Solid State Physics* (Thomson Learning, New York, 1976).

[28] N. Wetta and J.-C. Pain, Phys. Rev. B **100**, 205127 (2019).

[29] D. A. Liberman, Phys. Rev. B **20**, 4981 (1979).

[30] B. Wilson, V. Sonnad, P. Sterne, and W. Isaacs, J. Quant. Spectrosc. Radiat. Transfer **99**, 658 (2006).

[31] M. Pénicaud, J. Phys.: Condens. Matter **21**, 095409 (2009).

[32] B. F. Rozsnyai, Phys. Rev. A **5**, 1137 (1972).

[33] G. Massacrier, M. Böhme, J. Vorberger, F. Soubiran, and B. Militzer, Phys. Rev. Res. **3**, 023026 (2021).

[34] T. J. Callow, E. Kraisler, and A. Cangi, Phys. Rev. Res. **5**, 013049 (2023).

[35] B. Crowley and J. Harris, J. Quant. Spectrosc. Radiat. Transfer **71**, 257 (2001).

[36] F. Perrot and M. W. C. Dharma-wardana, Phys. Rev. E **52**, 5352 (1995).

[37] C. E. Starrett and D. Saumon, Phys. Rev. E **87**, 013104 (2013).

[38] C. E. Starrett and N. Shaffer, Phys. Rev. E **102**, 043211 (2020).

[39] T. Blenski and R. Piron, Phys. Rev. E **107**, 035209 (2023).

[40] P. Hohenberg and W. Kohn, Phys. Rev. **136**, B864 (1964).

[41] W. Kohn and L. J. Sham, Phys. Rev. **140**, A1133 (1965).

[42] N. Mermin, Phys. Rev. **137**, A1441 (1965).

[43] R. G. Parr and W. Yang, *Density-Functional Theory of Atoms and Molecules* (Oxford University Press, New York, 1989).

[44] A. F. Nikiforov, V. G. Novikov, and V. B. Uvarov, *Quantum-Statistical Models of Hot Dense Matter* (Birkauser, Basel, 2005).

[45] V. V. Karasiev, T. Sjostrom, J. Dufty, and S. B. Trickey, Phys. Rev. Lett. **112**, 076403 (2014).

[46] G. Faussurier, Phys. Plasmas **23**, 122704 (2016).

[47] J. Bruneau (private communication).

[48] N. F. Mott, Proc. Phys. Soc. A **62**, 416 (1949).

[49] C. E. Starrett, High Energy Density Phys. **16**, 18 (2015).

[50] C. Starrett, N. Gill, T. Sjostrom, and C. Greeff, Comput. Phys. Commun. **235**, 50 (2019).

[51] See Supplemental Material at http://link.aps.org/supplemental/10.1103/PhysRevB.108.085115 for a database containing isotherms of entropy at 0.01 electronvolt for elements of atomic number Z from 1 to 71.

[52] J. C. Slater, Phys. Rev. **81**, 385 (1951).

[53] R. van Leeuwen and E. J. Baerends, Phys. Rev. A **49**, 2421 (1994).

[54] S. Ichimaru, H. Iyetomi, and S. Tanaka, Phys. Rep. **149**, 91 (1987).

[55] L. Calderín, L. E. González, and D. J. González, J. Phys.: Condens. Matter **23**, 375105 (2011).

[56] J. Clérouin, C. Starrett, G. Faussurier, C. Blancard, P. Noiret, and P. Renaudin, Contrib. Plasma Phys. **52**, 17 (2012).

[57] V. N. Korobenko and A. D. Rakhel, Phys. Rev. B **85**, 014208 (2012).

[58] D. Li, H. Liu, S. Zeng, C. Wang, Z. Wu, P. Zhang, and J. Yan, Sci. Rep. **4**, 5898 (2014).

[59] D. V. Minakov, M. A. Paramonov, and P. R. Levashov, Phys. Rev. B **97**, 024205 (2018).

[60] P. M. Celliers, M. Millot, S. Brygoo, R. S. McWilliams, D. E. Fratanduono, J. R. Rygg, A. F. Goncharov, P. Loubeyre, J. H. Eggert, J. L. Peterson *et al.*, Science **361**, 677 (2018).

[61] D. Liu, W. Fan, L. Shan, C. Tian, B. Bi, F. Zhang, Z. Yuan, W. Wang, H. Liu, L. Yang *et al.*, Phys. Plasmas **26**, 122705 (2019).

[62] D. Liu, W. Fan, L. Shan, F. Wang, M. Shui, B. Zhu, Y. Wu, F. Zhang, B. Bi, C. Tian *et al.*, AIP Adv. **10**, 095008 (2020).

[63] L. Lewin, *Polylogarithms and Associated Functions* (Elsevier North Holland, Amsterdam, 1981).

[64] D. F. Connon, arXiv:0710.4022 (2008).